LINEAR SOURCE METHOD OF CHARACTERISTICS IN HELIOS2

Charles A. Wemple and Rodolfo M. Ferrer

Studsvik Scandpower, Inc., 1070 Riverwalk Drive, Suite 150, Idaho Falls, ID 83402, USA

charles.wemple@studsvik.com, rodolfo.ferrer@studsvik.com

doi.org/10.13182/PHYSOR22-37242

ABSTRACT

The HELIOS2 lattice code has been extended with the development of a linear source Method of Characteristics option. The linear source equations are derived within the scope of the HELIOS2 general geometry and non-cyclic ray tracing. The implementation was tested for fine and coarse spatial mesh models of the 2D C5G7 MOX computational benchmark, which provides a pure and extreme test of a transport solver. The linear source yields at least comparable accuracy with reduced computational resource requirements relative to the flat-source approximation.

KEYWORDS: Linear source, MoC, HELIOS, deterministic transport

1. INTRODUCTION

The Studsvik Scandpower code HELIOS2 [1] is a fast lattice transport code that has gained wide use for reactor fuel cycle analysis in commercial, regulatory, and research environments. It contains two transport solvers – Collision Probabilities (CP) and Method of Characteristics (MoC) – with a general geometry modeling capability and generalized depletion for a variety of fuel types, experimental facilities, and isotope production applications. Nuclear data libraries are derived primarily from ENDF/B-VIIR1 [2] data, supplemented with JENDL-4.0 [3], TENDL-2014 [4], and TENDL-2015 [5] to complete the depletion chains. Coupled with the input pre-processor AURORA and output processor ZENITH, it forms a powerful and flexible system for a wide variety of commercial and research nuclear applications.

In the past several years, many methodological improvements have been made in the HELIOS2 lattice code, focusing on the MoC transport solver. These improvements include implementing the Chebyshev Rational Approximation Method (CRAM) for depletion [6], an unstructured partial-current coarse mesh finite difference (upCMFD) acceleration scheme [7], an XSUSA-based uncertainty propagation method [8], anisotropic scattering source option, and OpenMP multithreading. The most recent improvement is the addition of a linear source method, based on the methodology defined for the CASMO5 lattice code [9-11].

2. THEORY

The standard flat-source MoC definition can accurately represent the angular flux at the various region boundary surfaces. However, for many common components of reactors, the flat-source assumption requires a fine spatial segmentation, which can place an excessive modelling burden on the user and require significant computational resources to perform the resulting calculation. Relaxing the flat-source assumption in favor of a linearly varying source in each mesh along each track can alleviate this burden, by

permitting a coarser spatial segmentation while retaining the original solution accuracy. This section outlines the derivation of the linear source MoC as implemented in HELIOS2; the general geometry and consequent lack of cyclic ray tracing produce a slightly different formulation than other implementations.

2.1. Angular Flux Moments

The differential form of the Boltzmann transport equation along a distance s_m in direction m (a double index for the azimuthal direction a and polar direction p) within a region i is given by:

$$\frac{d\psi^g_{m,i}}{ds_m} + \Sigma^g_{tr,i}\psi^g_{m,i} = q^g_{m,i}(s_m) \tag{1}$$

where $\psi^g_{m,i}$ is the angular flux, $\Sigma^g_{\mathrm{tr,i}}$ is the transport cross section, and the linear source along the track length s_m is assumed to be represented as:

$$q^g_{m,i}(s_{m,i}) = \bar{q}^g_{m,i} + \hat{q}^g_{m,i}(s_m - s^c_{m,i}) \tag{2}$$

with $s^c_{m,i} = s_{m,i}/2$ and the expansion coefficients $\bar{q}_{m,i}$ and $\hat{q}_{m,i}$ defined later. Inserting this formulation into Eq. (1) and integrating along the track length in region i yields the characteristics equation:

$$\psi^g_{m,i}(s_m) = \psi^g_{m,i}(0) + \left(\frac{\bar{q}^g_{m,i}}{\Sigma^g_{tr,i}} - \psi^g_{m,i}(0)\right)F_1(\tau^g_m) + \frac{\hat{q}^g_{m,i}}{2\left(\Sigma^g_{tr,i}\right)^2}F_2(\tau^g_m) \tag{3}$$

with the variable optical thickness $\tau_m = \Sigma^g_{\mathrm{tr,i}} s_m$ and the functions F_1 and F_2 defined by:

$$F_1(\tau^g_m) = 1 - e^{-\tau^g_m} \tag{4}$$

$$F_2(\tau^g_m) = 2(\tau^g_m - F_1(\tau^g_m)) - \tau^g_{m,i}F_1(\tau^g_m)\ . \tag{5}$$

The average and first-order spatial moment of the angular flux along a given track distance are defined as:

$$\bar{\psi}^g_{m,i} = \frac{1}{s_{m,i}}\int_0^{s_{m,i}} \psi^g_{m,i}(s'_m)\,ds'_m \tag{6}$$

$$\hat{\psi}^g_{m,i} = \frac{1}{s_{m,i}}\int_0^{s_{m,i}} s'_m\psi^g_{m,i}(s'_m)\,ds'_m \tag{7}$$

Applying the integration in Eq. (6) to Eq. (1) produces the balance equation:

$$\frac{\psi^g_{m,i}(s_{m,i}) - \psi^g_{m,i}(0)}{s_{m,i}} + \Sigma^g_{tr,i}\bar{\psi}^g_{m,i} = \bar{q}^g_{m,i} \tag{8}$$

with the angular fluxes given by Eq. (3). Applying the integration in Eq. (7) to Eq. (3) gives the first moment of the angular flux:

$$\hat{\psi}^g_{m,i} = \psi^g_{m,i}(0)s^c_{m,i} + \left(\frac{\bar{q}^g_{m,i}}{\Sigma^g_{tr,i}} - \psi^g_{m,i}(0)\right)\frac{G_1\left(\tau^g_{m,i}\right)}{\Sigma^g_{tr,i}} + \frac{\hat{q}^g_{m,i}}{2\left(\Sigma^g_{tr,i}\right)^2}s_{m,i}G_2\left(\tau^g_{m,i}\right) \tag{9}$$

with the functions G_1 and G_2 defined as:

$$G_1(\tau^g_{m,i}) = 1 + \frac{\tau^g_{m,i}}{2} - \left(1 + \frac{1}{\tau^g_{m,i}}\right)F_1(\tau^g_{m,i}) \tag{10}$$

$$G_2(\tau^g_{m,i}) = \frac{\tau^g_{m,i}}{6} - 2\left(1 + \frac{1}{\tau^g_{m,i}}\right) + \left(1 + \frac{1}{\tau^g_{m,i}}\right)\left(1 + \frac{2}{\tau^g_{m,i}}\right)F_1(\tau^g_{m,i}) \ . \tag{11}$$

2.2. Track-based Integrations

It is convenient to introduce a generic integration of two direction-dependent functions, $f_{m,i}$ and $g_{m,i}$:

$$\langle f, g\rangle_{m,i} = \frac{\sin\theta_p}{V_i}\sum_k \int_0^{t_{m,k,i}} f_{m,k,i}(t'_m)g_{m,k,i}(t'_m)dt'_m\delta A_a \ , \tag{12}$$

where the index k denotes an individual track, θ_p is the polar angle, V_i is the region volume, and δA_a is the width of a characteristic ray. In order to conserve volume-integrated quantities, the scaled track length $t_{m,k,i}=\xi_i s_{m,k,i}$ has been substituted for the track length $s_{m,k,i}$, with the scaling factor ξ_i defined as the ratio of the true region volume to the track-integrated region volume. For truly rigorous particle conservation in the case of anisotropic scattering, the scaling factor should also be a function of direction [11]. However, the fine angular quadrature employed in HELIOS2, similar to that used in CASMO5 [9-11], reduces the inconsistencies to negligible levels. For isotropic functions f and g, the integral in Eq. (12) reduces to:

$$\langle f, g\rangle_i = 4\pi\sum_m \omega_m \langle f, g\rangle_{m,i} \ . \tag{13}$$

where ω_m is the quadrature weight for direction $m=(a,p)$, with a the azimuthal and p the polar angle.

2.3. Local Coordinate System

To formulate a linearly varying source within each spatial region more easily, a local coordinate system ($x = X - X^c_i$; $y = Y - Y^c_i$) is introduced. The "numerical centroid" in region i, (X^c_i, Y^c_i), is defined by:

$$X^c_i = \left\langle 1, \frac{1}{4\pi}X\right\rangle_i \quad , \quad Y^c_i = \left\langle 1, \frac{1}{4\pi}Y\right\rangle_i \tag{14}$$

where the coordinates (X,Y) are related to the scaled track length by:

$$\begin{aligned} X(t_m) &= \cos\varphi_a \sin\theta_p \frac{t_m}{\xi_i} + X^{in}_{a,k,i} \\ Y(t_m) &= \sin\varphi_a \sin\theta_p \frac{t_m}{\xi_i} + Y^{in}_{a,k,i} \end{aligned} \tag{15}$$

Applying Eq. (13), the track-based computation of the centroids, which must be isotropic, become:

$$\begin{aligned} X_i^c &= \frac{1}{V_i}\sum_a \omega_a \delta A_a \sum_k X_{a,k,i}^{in} t_{a,k,i} \\ Y_i^c &= \frac{1}{V_i}\sum_a \omega_a \delta A_a \sum_k Y_{a,k,i}^{in} t_{a,k,i} \end{aligned} \tag{16}$$

where $t_{a,k,i} = \sin\theta_p t_{m,k,i}$.

2.4. Region-averaged Flux and Source

Now, consider a spatially linear scalar flux and isotropic source in the local coordinate system of region i:

$$\phi_i^g(x,y) = \bar{\phi}_i^g + \Phi_{i,x}^g x + \Phi_{i,y}^g y \tag{17}$$

$$q_i^g(x,y) = \frac{1}{4\pi}(\bar{q}_i^g + q_{i,x}^g x + q_{i,y}^g y) \tag{18}$$

The flux moments in Eq. (17) may be defined by applying $\langle 1,\psi^g\rangle_i$, $\langle x,\psi^g\rangle_i$, and $\langle y,\psi^g\rangle_i$:

$$\bar{\phi}_i^g = \frac{4\pi}{V_i}\sum_m \omega_m \sin\theta_p \delta A_a \sum_k \bar{\psi}_{m,k,i}^g t_{m,k,i} \tag{19}$$

$$\Phi_{i,x}^g = \frac{4\pi}{V_i}\sum_m \omega_m \sin\theta_p \delta A_a \sum_k \left(\frac{\cos\varphi_a \sin\theta_p \bar{\psi}_{m,k,i}^g}{\xi_i} + x_{a,k,i}^{in} \bar{\psi}_{m,k,i}^g \right) t_{m,k,i} \tag{20}$$

$$\Phi_{i,y}^g = \frac{4\pi}{V_i}\sum_m \omega_m \sin\theta_p \delta A_a \sum_k \left(\frac{\sin\varphi_a \sin\theta_p \bar{\psi}_{m,k,i}^g}{\xi_i} + y_{a,k,i}^{in} \bar{\psi}_{m,k,i}^g \right) t_{m,k,i} \ . \tag{21}$$

Similarly, the source coefficients in Eq. (18) are defined by applying $\langle 1,q^g\rangle_i$, $\langle x,q^g\rangle_i$, and $\langle y,q^g\rangle_i$:

$$\begin{aligned} \langle 1, q^g \rangle_i &= \bar{q}_i^g \\ \langle x, q^g \rangle_i &= q_{i,x}^g M_{xx,i} + q_{i,y}^g M_{xy,i} \\ \langle y, q^g \rangle_i &= q_{i,x}^g M_{yx,i} + q_{i,y}^g M_{yy,i} \end{aligned} \ , \tag{22}$$

where the coefficients M are defined by:

$$M_{xx,i} = \frac{1}{V_i}\sum_a \bar{\omega}_a \sum_k \left(\frac{\left(\cos\varphi_a s_{a,k,i}\right)^2}{3} + x_{a,k,i}^{in} x_{a,k,i}^{out} \right) t_{a,k,i} \tag{23}$$

$$M_{xy,i} = \frac{1}{V_i}\sum_a \bar{\omega}_a \sum_k \left(\frac{\sin\varphi_a \cos\varphi_a}{3} s_{a,k,i}^2 + \frac{x_{a,k,i}^{in} y_{a,k,i}^{out} + x_{a,k,i}^{out} y_{a,k,i}^{in}}{2} \right) t_{a,k,i} \tag{24}$$

$$M_{yy,i} = \frac{1}{V_i}\sum_a \bar{\omega}_a \sum_k \left(\frac{\left(\sin\varphi_a s_{a,k,i}\right)^2}{3} + y^{in}_{a,k,i} y^{out}_{a,k,i} \right) t_{a,k,i} \tag{25}$$

with $s_{a,k,i} = \sin\theta_p s_{m,k,i}$ and $\bar{\omega}_a = \omega_a \delta A_a$, and $M_{yx,i} = M_{xy,i}$. The linear source components of Eq. (22) are related to the flux and source moments by:

$$\begin{bmatrix} 1 & 0 & 0 \\ 0 & M_{xx,i} & M_{xy,i} \\ 0 & M_{xy,i} & M_{yy,i} \end{bmatrix} \begin{bmatrix} \bar{q}^g_i \\ q^g_{i,x} \\ q^g_{i,y} \end{bmatrix} = \begin{bmatrix} \bar{q}^g_i \\ Q^g_{i,x} \\ Q^g_{i,y} \end{bmatrix} = \frac{1}{4\pi}\sum_{g'} \left(\Sigma^{g'\to g}_{s,i} + \frac{\chi^g}{k^\infty} \nu\Sigma^{g'}_{f,i} \right) \begin{bmatrix} \bar{\phi}^{g'}_i \\ \Phi^{g'}_{i,x} \\ \Phi^{g'}_{i,y} \end{bmatrix}. \tag{26}$$

Now, the linear source coefficients of Eq. (2) may be defined by applying Eq. (18), yielding:

$$\begin{aligned} \bar{q}^g_{m,k,i} &= \frac{1}{4\pi}\left(\bar{q}^g_i + q^g_{i,x} x^c_{a,k,i} + q^g_{i,y} y^c_{a,k,i}\right) \\ \hat{q}^g_{m,i} &= \frac{1}{4\pi}\frac{\left(\cos\varphi_a \sin\theta_p q^g_{i,x} + \sin\varphi_a \sin\theta_p q^g_{i,y}\right)}{\xi_i} \end{aligned}. \tag{27}$$

Combining the linear source coefficients above with Eq. (8) and Eq. (9), the flux moments of Eqs. (19)-(21), and substituting $\Delta^g_{m,k,i} = \psi^g_{m,k,i}(0) - \psi^g_{m,k,i}(s_{m,k,i})$, gives the final track-based form of the flux moments:

$$\bar{\phi}^g_i = \frac{\bar{q}^g_i}{\Sigma^g_{tr,i}} + \frac{4\pi}{\Sigma^g_{tr,i} V_i}\sum_a \bar{\omega}_a \sum_p \bar{\omega}_p \Delta^g_{m,k,i} \tag{28}$$

$$\begin{aligned} \Phi^g_{i,x} = {} & \frac{q^g_{i,x}}{\Sigma^g_{T,i}} C^g_{i,x} + \frac{q^g_{i,y}}{\Sigma^g_{T,i}} C^g_{i,xy} + \frac{\bar{q}^g_i}{\Sigma^g_{T,i} V_i}\sum_a \bar{\omega}_a \sum_p \bar{\omega}_p \frac{1}{\Sigma^g_{T,i}} \sum_k G_1\left(\tau^g_{m,k,i}\right) \cos\varphi_a s_{a,k,i} \\ & + \frac{4\pi}{\Sigma^g_{T,i} V_i}\sum_a \bar{\omega}_a \sum_p \bar{\omega}_p \left(\sum_k \psi^g_{m,k,i}(0) H_1\left(\tau^g_{m,k,i}\right) \cos\varphi_a s_{a,k,i} + \sum_k x^{in}_{a,k,i} \Delta^g_{m,k,i} \right) \end{aligned} \tag{29}$$

$$\begin{aligned} \Phi^g_{i,y} = {} & \frac{q^g_{i,x}}{\Sigma^g_{T,i}} C^g_{i,yx} + \frac{q^g_{i,y}}{\Sigma^g_{T,i}} C^g_{i,y} + \frac{\bar{q}^g_i}{\Sigma^g_{T,i} V_i}\sum_a \bar{\omega}_a \sum_p \bar{\omega}_p \frac{1}{\Sigma^g_{T,i}} \sum_k G_1\left(\tau^g_{m,k,i}\right) \sin\varphi_a s_{a,k,i} \\ & + \frac{4\pi}{\Sigma^g_{T,i} V_i}\sum_a \bar{\omega}_a \sum_p \bar{\omega}_p \left(\sum_k \psi^g_{m,k,i}(0) H_1\left(\tau^g_{m,k,i}\right) \sin\varphi_a s_{a,k,i} + \sum_k y^{in}_{a,k,i} \Delta^g_{m,k,i} \right) \end{aligned} \tag{30}$$

where $\bar{\omega}_p = \omega_p \sin\theta_p$, the coefficients C are given by:

$$C^g_{i,x} = \frac{1}{\Sigma^g_{T,i} V_i}\sum_a \bar{\omega}_a \sum_p \bar{\omega}_p \sum_k \cos\varphi_a s_{a,k,i} \left[x^c_{a,k,i} G_1\left(\tau^g_{m,k,i}\right) + \frac{\cos\varphi_a s_{a,k,i}}{2} G_2\left(\tau^g_{m,k,i}\right) \right] + \frac{1}{V_i}\sum_a \bar{\omega}_a \sum_k x^{in}_{a,k,i} x^c_{a,k,i} t_{a,k,i} \tag{31}$$

$$C^g_{i,xy} = \frac{1}{\Sigma^g_{T,i} V_i}\sum_a \bar{\omega}_a \sum_p \bar{\omega}_p \sum_k \cos\varphi_a s_{a,k,i} \left[y^c_{a,k,i} G_1\left(\tau^g_{m,k,i}\right) + \frac{\sin\varphi_a s_{a,k,i}}{2} G_2\left(\tau^g_{m,k,i}\right) \right] + \frac{1}{V_i}\sum_a \bar{\omega}_a \sum_k x^{in}_{a,k,i} y^c_{a,k,i} t_{a,k,i} \tag{32}$$

$$C^g_{i,yx} = \frac{1}{\Sigma^g_{T,i} V_i} \sum_a \bar{\omega}_a \sum_p \bar{\omega}_p \sum_k \sin\varphi_a s_{a,k,i} \left[x^c_{a,k,i} G_1\left(\tau^g_{m,k,i}\right) + \frac{\cos\varphi_a s_{a,k,i}}{2} G_2\left(\tau^g_{m,k,i}\right) \right] + \frac{1}{V_i} \sum_a \bar{\omega}_a \sum_k y^{in}_{a,k,i} x^c_{a,k,i} t_{a,k,i} \quad (33)$$

$$C^g_{i,y} = \frac{1}{\Sigma^g_{T,i} V_i} \sum_a \bar{\omega}_a \sum_p \bar{\omega}_p \sum_k \sin\varphi_a s_{a,k,i} \left[y^c_{a,k,i} G_1\left(\tau^g_{m,k,i}\right) + \frac{\sin\varphi_a s_{a,k,i}}{2} G_2\left(\tau^g_{m,k,i}\right) \right] + \frac{1}{V_i} \sum_a \bar{\omega}_a \sum_k y^{in}_{a,k,i} y^c_{a,k,i} t_{a,k,i} \quad (34)$$

and the function H_1 is defined as:

$$H_1(\tau^g_{m,k,i}) = \frac{\tau^g_{m,k,i}}{2} - G_1(\tau^g_{m,k,i}) . \quad (35)$$

The HELIOS2 implementation applies the upCMFD acceleration to the linear source MoC. This mode has been shown [12, 13] to be unconditionally stable in 1D slab geometry for the Step Characteristic and Linear Characteristic schemes. The issue of particle conservation has been addressed in the literature [11].

3. RESULTS

Testing of the linear source implementation was performed with the 2D C5G7 MOX benchmark [14]. This is a computational benchmark developed by the NEA Nuclear Science Committee as a test case for lattice physics computational tools; it consists of a one-quarter core 2x2 array of 17x17 MOX and UO2 fuel bundles with a surrounding moderator/reflector. The system uses reflected boundary conditions on the top and left, vacuum boundaries on the bottom and right, and is infinite axially. The pin pitch is 1.26cm, the fuel pin outer radius is 0.54cm, and the reflector thickness is the same as one fuel bundle. A seven-group, transport-corrected, isotropic scattering cross section set for each homogenized material (four fuel types – UO2 and three MOX types - water hole, fission chamber, moderator) was supplied for use in the computation; this eliminates any dependencies on cross section libraries and provides a pure and extreme test of a lattice physics solver. The core layout is shown in Figure 1, along with the reference Monte Carlo relative fission rate distribution (k_∞=1.18655) provided in the benchmark.

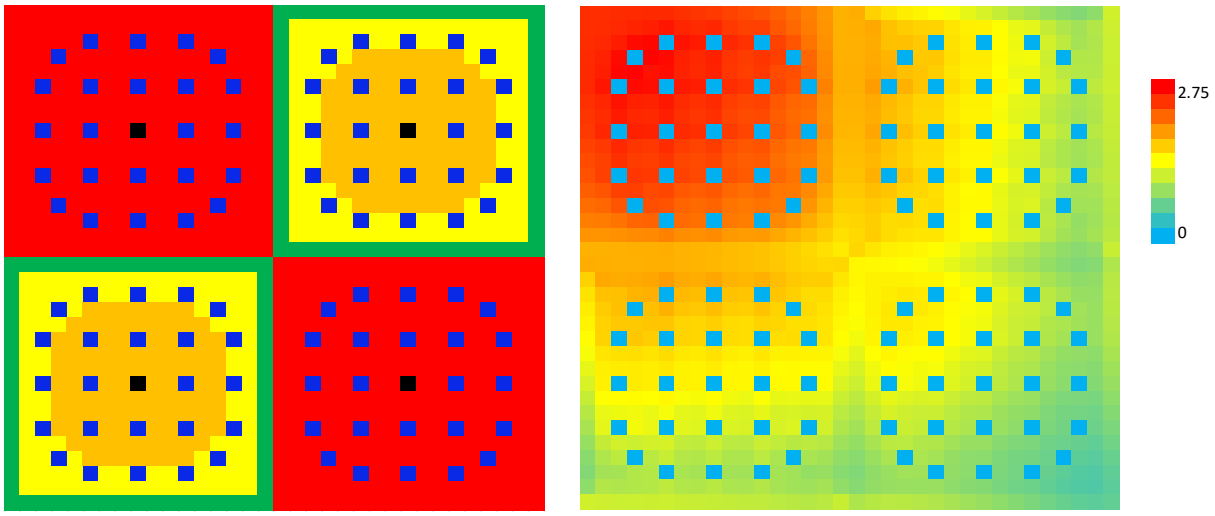

Figure 1. Fuel assembly layout (left) and relative fission rate distribution (right) of C5G7 MOX benchmark. Red=UO_2 fuel, green=4.3% MOX fuel, yellow=7.0% MOX fuel, orange=8.7% MOX fuel, blue=guide tube, black=fission chamber/instrumentation tube.

As shown in Figure 2, two models were constructed – one with a fine spatial mesh to give the best results from the flat-source approximation, and one with a coarse spatial mesh to demonstrate the effects of the linear-source approximation. The goal was to achieve comparable eigenvalue results from the linear-source coarse mesh model with the flat-source fine mesh model. Calculations were run using both flat-source and linear-source approximations for each model, with k_∞ and pin-wise relative fission rates edited for all cases. All cases used 48 azimuthal angles and 3 polar angles. The fine mesh model used a minimum ray spacing of 0.01cm, while the coarse mesh model used a minimum ray spacing of 0.03cm.

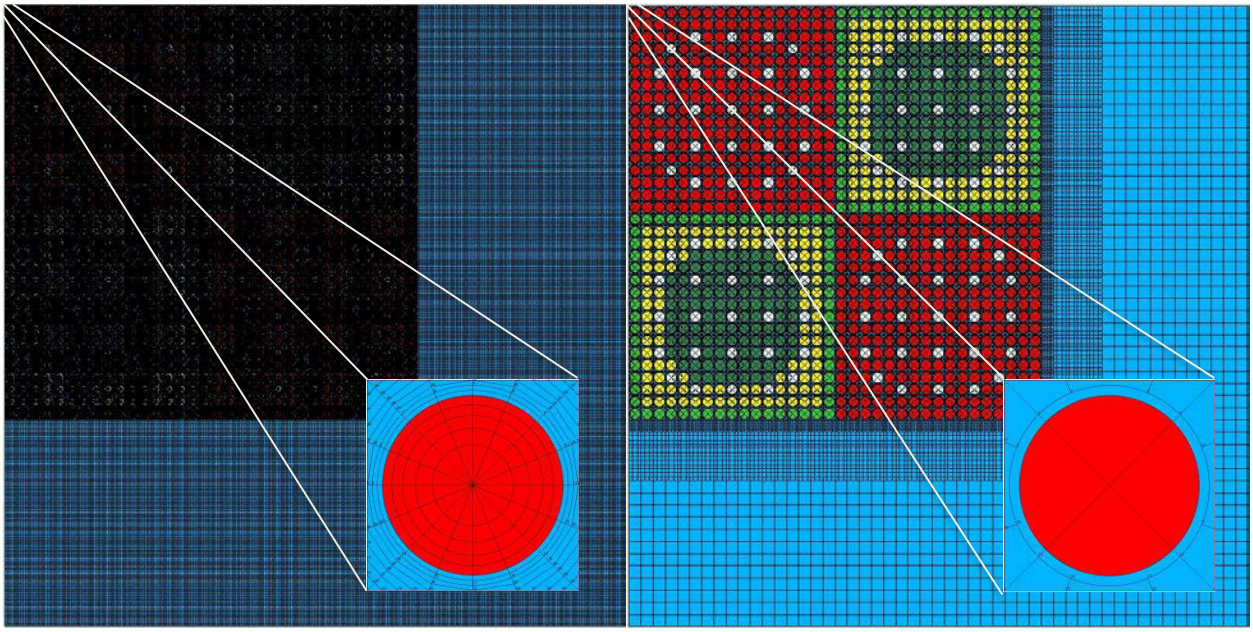

Figure 2. C5G7 MOX benchmark core and pin models – fine mesh (left) and coarse mesh (right).

A summation of the results is presented in Table I. The linear source results demonstrate the benefits of this methodology in MoC calculations. The linear source provides improved results for identical mesh definitions with an increased computational cost but, by permitting accurate calculations with a coarser region mesh, can achieve equivalent or better results at a fraction of the computational and modeling burden.

Table I. Integral results of C5G7 MOX benchmark calculations.

Quantity		Flat source		Linear source	
		Fine mesh	Coarse mesh	Fine mesh	Coarse mesh
k_∞		1.186564	1.186224	1.186632	1.186590
Δk (pcm) from benchmark		1.4	-32.6	8.2	4.0
Relative fission rate errors (%)	Max	1.102	1.347	0.799	0.928
	Min	-0.405	-0.601	-0.574	-0.600
	Avg	0.1711	0.2850	0.1419	0.1778
	RMS	0.2512	0.3595	0.2001	0.2252
Relative CPU time		1.0	0.12	2.79	0.30
Relative memory		1.0	0.16	1.93	0.30
Number of regions		255476	29348	255476	29348
Number of tracks		447311	171617	447311	171617

Figure 3 displays the relative fission rate percent differences for the two fine mesh calculations. The linear source calculation produces improved results, with a noticeable reduction in the largest errors throughout the distribution. The linear source case reduces both the average and RMS fission rate errors, compared to the flat source results. It is interesting to note that both models tend to overpredict the fission rate for the peripheral pins, where the thermal flux gradients are strong, although the linear source differences are smaller than the flat source differences.

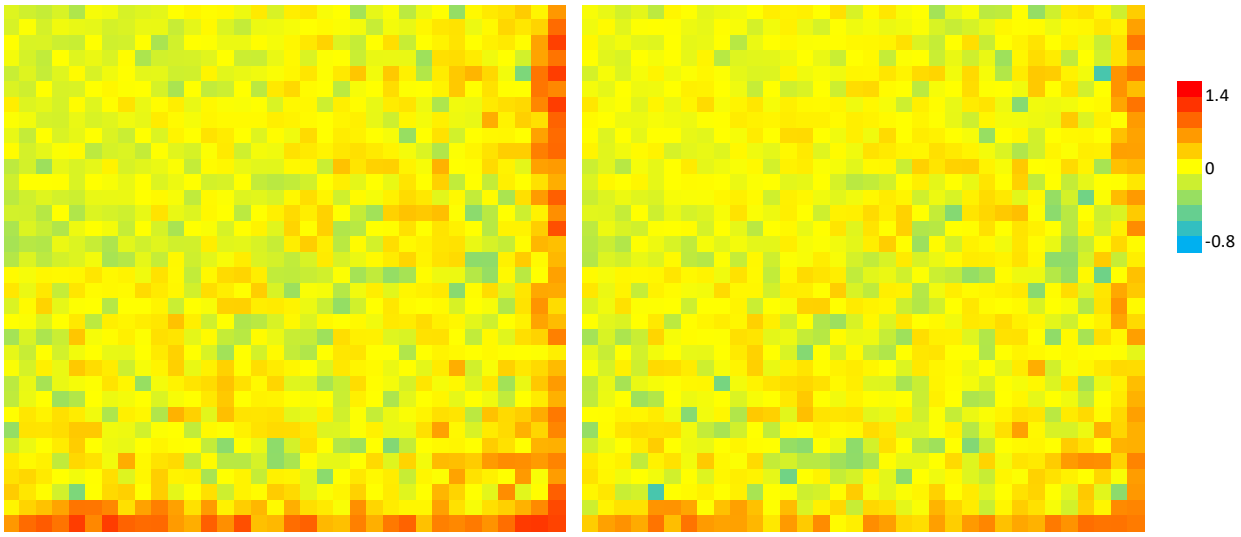

Figure 3. HELIOS2 relative fission rate differences (%) from reference for fine mesh model calculations – flat source (left) and linear source (right).

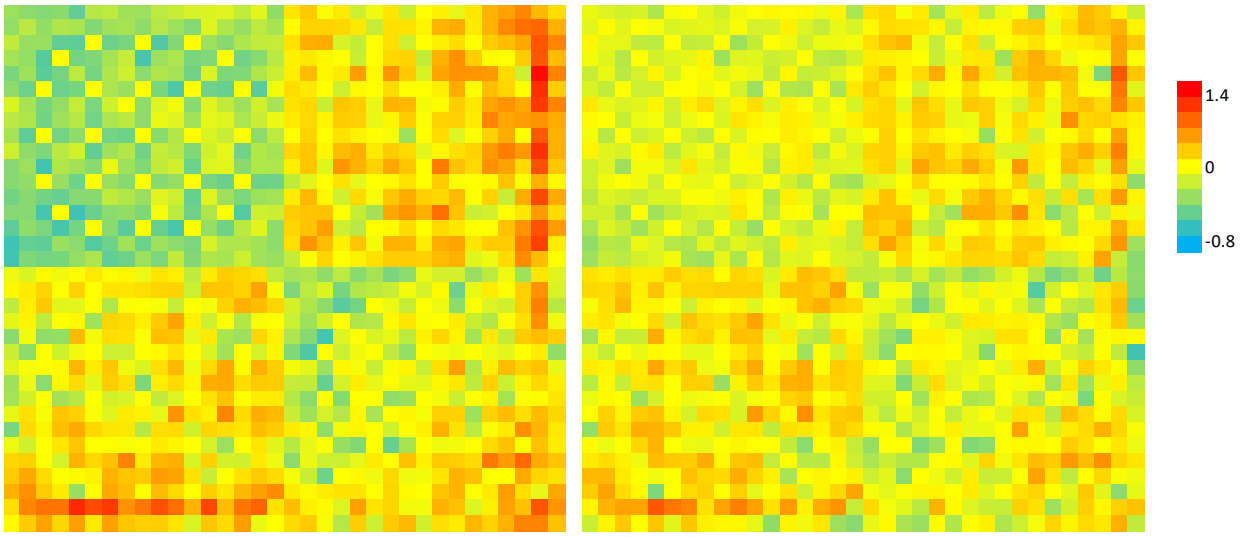

Figure 4. HELIOS2 relative fission rate differences (%) from reference for coarse mesh model calculations – flat source (left) and linear source (right).

Figure 4 displays the relative fission rate percent differences for the two coarse mesh calculations. The flat source results display large differences in regions with strong flux gradients, especially near the guide tubes and in the MOX assemblies; these differences are substantially reduced by application of the linear source

model. The tendency of the coarse mesh to overpredict fission rates in the MOX bundles and underpredict in the UO_2 bundles is also reduced in the linear source results. The coarse mesh linear source results, both k_∞ and fission rate distribution, are comparable to the fine mesh flat source results, but are achieved with only 30% of the CPU time and 30% of the computer memory.

4. CONCLUSIONS

A linear source extension of the Method of Characteristics has been derived for, and implemented in, the HELIOS2 two-dimensional lattice code. Test calculations with the 2D C5G7 MOX benchmark demonstrate the efficacy of this new calculation option. The linear source provides increased solution accuracy with existing spatial meshing schemes or provides comparable accuracy with a substantially reduced spatial mesh definition, thus requiring reduced computational resources. The linear source extension has also been applied to the anisotropic scattering treatment (up to P3) in the latest version of HELIOS2.

REFERENCES

1. C.A. Wemple, H-N.M. Gheorghiu, R.J.J. Stamm'ler, E.A. Villarino, "Recent Advances in the HELIOS-2 Lattice Physics Code," *Proceedings of PHYSOR 2008*, Interlaken, CH, September 14-19, 2008.
2. M.B. Chadwick, et al., "ENDF/B-VII.1 Nuclear Data for Science and Technology: Cross Sections, Covariances, Fission Product Yields and Decay Data," *Nuclear Data Sheets* **112**(12), pp. 2887-2996 (2011).
3. K. Shibata, et al., "JENDL-4.0: A New Library for Nuclear Science and Technology," *J. Nucl. Sci. Technol.* **48**(1), pp. 1-30 (2011).
4. M. Fleming, J.C. Sublet, J. Kopecky, D. Rochman, A.J. Koning, "Probing experimental and systematic trends of the neutron-induced TENDL-2014 nuclear data library", *UKAEA-R(15)29*, UK Atomic Energy Authority, October 2015.
5. J.Ch. Sublet, A.J. Koning, D. Rochman, M. Fleming, M. Gilbert, "TENDL-2015: Delivering Both Completeness and Robustness", *Advances in Nuclear Nonproliferation Technology and Policy Conference*, Santa Fe, NM, USA, Sept. 25-30, 2016.
6. C. Wemple, T. Simeonov, "Advances in HELIOS2 Nuclear Data Library," *Kerntechnik*, **82**(4), pp. 445-447 (2017).
7. C. Wemple, T. Simeonov, "HELIOS2 Verification and Benchmark Testing," *28th AER Symposium on VVER Reactor Physics and Reactor Safety*, Olomouc, CZ, Oct 8-12, 2018.
8. C. Wemple, W. Zwermann, "Nuclear data uncertainty propagation by the XSUSA method in the HELIOS2 lattice code," *Proceedings of ND 2016: International Conference on Nuclear Data for Science and Technology*, EPJ Web of Conferences, **146**, 02020 (2017).
9. R. Ferrer, J. Rhodes, K. Smith, "Linear Source Approximation in CASMO5," *Proceedings of PHYSOR 2012 – Advances in Reactor Physics*, Knoxville, TN, USA, April 15-20, 2012.
10. R.M. Ferrer, J.D. Rhodes III, "A Linear Source Approximation Scheme for the Method of Characteristics," *Nucl. Sci. Eng.* **182**, pp. 151-165 (2016).
11. R.M. Ferrer, J.D. Rhodes III, "The Linear Source Approximation and Particle Conservation in the Method of Characteristics for Isotropic and Anisotropic Sources," *Ann. Nucl. Energy* **115**, pp. 209-219 (2018).
12. N.Z. Cho, G.S. Lee, C.J. Park, "Partial current-based CMFD acceleration of the 2D/1D fusion method for 3D whole-core transport calculations," *Trans. Am. Nucl. Soc.* **88**, p. 594 (2003).
13. R.M. Ferrer, "Stability analysis of coarse-mesh finite difference acceleration schemes and moment-based, spatially-linear discretizations," *Ann. Nucl. Energy* **158**, 108280 (2021).
14. E.E. Lewis, M.A. Smith, N. Tsoulfanidis, G. Palmiotti, T.A. Taiwo, R.N. Blomquist, "Benchmark specification for Deterministic 2-D/3-D MOX fuel assembly transport calculations without spatial homogenization," *NEA/NSC/DOC(2001)4*, Nuclear Energy Agency, 2001.